Technology Update

Algorithms to Improve the Reparameterization of Spherical Mappings of Brain Surface Meshes

Rachel A. Yotter, PhD, Paul M. Thompson, PhD, Christian Gaser, PhD

From the Department of Psychiatry, Friedrich-Schiller University, Jena, Germany (RAY, CG); Laboratory of Neuro Imaging, Department of Neurology, Division of Brain Mapping, UCLA School of Medicine, Los Angeles, California (PMT).

ABSTRACT

A spherical map of a cortical surface is often used for improved brain registration, for advanced morphometric analysis (eg, of brain shape), and for surface-based analysis of functional signals recorded from the cortex. Furthermore, for intersubject analysis, it is usually necessary to reparameterize the surface mesh into a common coordinate system. An isometric map conserves all angle and area information in the original cortical mesh; however, in practice, spherical maps contain some distortion. Here, we propose fast new algorithms to reduce the distortion of initial spherical mappings generated using one of three common spherical mapping methods. The algorithms iteratively solve a nonlinear optimization problem to reduce distortion. Our results demonstrate that our correction process is computationally inexpensive and the resulting spherical maps have improved distortion metrics. We show that our corrected spherical maps improve reparameterization of the cortical surface mesh, such that the distance error measures between the original and reparameterized surface are significantly decreased.

Keywords: Spherical mapping, surface mesh, distortion, intersubject analysis, parameterization.

Acceptance: Received November 12, 2009, and in revised form February 23, 2010. Accepted for publication February 27, 2010.

Correspondence: Address correspondence to Rachel A. Yotter, Department of Psychiatry, Friedrich-Schiller University, 3 Jahnstrasse, 07743 Jena, Germany. E-mail: rachel.yotter@uni-jena.de

Conflict of Interest: The authors declare no conflicts of interests.

J Neuroimaging 2010;XX:1-14.
DOI: 10.1111/j.1552-6569.2010.00484.x

Introduction

Most brain MRI scanning protocols acquire volumetric data about the anatomy of the subject. However, it is sometimes desirable to conduct analyses that focus exclusively on the geometry of the cortical surface. This type of analysis may be conducted directly in volume space or by first generating a surface mesh from the volumetric data.[1-3] A surface mesh is useful for computing average surfaces, and the surface coordinates are useful for making comparisons of data across subjects that take into account the cortical folding pattern. Furthermore, a surface mesh makes it easier to perform some types of shape analyses, for example, spherical harmonic analysis, Laplace–Beltrami (LB) eigenmaps (another form of shape analysis), gyrification indices that measure surface complexity in 3-dimensional (3D), and complexity analysis that regrids the cortex.[4-6] To proceed with these analyses, a surface mesh that accurately represents cortical anatomy must first be generated.

Surface analyses have special advantages that are not present using volumetric data alone. For instance, brain surface meshes have been shown to increase the accuracy of brain registration compared with linear Talairach registration.[7-10] Brain surface meshes also permit new forms of analyses, such as gyrification indices that measure surface complexity in 3D,[6,11,12] cortical thickness,[13,14] and data compression and searching in mining databases.[15] Furthermore, inflation or spherical mapping of the cortical surface mesh raises the buried sulci to the surface so that mapped functional activity in these regions can be easily visualized. However, the primary purpose behind spherical mapping of the brain surface mesh is to generate a common coordinate system for intersubject analysis. To place a subject into a common coordinate system, the surface mesh usually must be reparameterized.

One valuable type of spherical map is a pseudo-isometric map, which attempts to conserve both angle and area information from the cortical surface mesh. Any mapping may retain area information by computing the Jacobian; however, a pseudo-isometric map preserves the local areas as much as possible, such that measuring relative areas in the sphere is essentially the same as doing so on the original surface, without having to know the Jacobian of the mapping.

Because of the highly folded nature of the cortical surface, however, it is not possible to obtain a perfectly isometric spherical map of the cortical surface mesh. In addition, depending on the priorities of the application, either angle or area preservation must be optimized at the expense of the other. However, it has not been explored which metric most influences the accuracy of reparameterization. It is hypothesized that area distortion is more important than angular distortion. Because there are an infinite number of solutions for an equiareal mapping, it can

be advantageous to choose a solution that also keeps angular distortion at a minimum.[16]

Previously, most efforts to minimize distortion concurred with the algorithms used to generate the initial spherical mapping. For instance, one can create a conformal, or angle-preserving, spherical mapping. There is some evidence that conformal maps may exist in the V1 visual cortex for processing visual data.[17] Also, it may be easier to solve partial differential equations on a grid if the grid is conformal, such as for signal smoothing or for surface-to-surface registration applications. A conformal map of a surface mesh can be generated by either solving a partial differential equation that involves the LB operator of the surface coordinates,[18,19] often using sulcal features as explicit landmark constraints,[20-22] or by minimizing the harmonic energy of the mapping to the sphere using variational methods.[23-26] Another quasi-conformal mapping procedure uses circle packing as a discrete approximation to the classical continuous mapping theory.[27] More recently, some researchers have used a branch of differential geometry known as the exterior calculus to build conformal grids directly on surfaces, using holomorphic differential one-forms.[28] Conformal grids on surfaces may also be generated using diverse methods such as the Ricci flow method,[29,30] algebraic function theory,[31] slit mapping,[32] and cohomology theory.[28] The resulting conformal grids may be used for shape analysis using Teichmuller space theory or tensor-based morphometry on the surface metric.[28,33]

Alternatively, specific landmark features, such as sulcal curves lying in the cortex, can be forced to map to designated locations on the sphere, using either covariate partial differential equations derived from linear elasticity,[34] level set methods and implicit function theory,[35] or approximately, by using mutual information defined on surfaces.[24,36] Although some approaches have computed surface-to-surface registrations by intermediate mappings of both surfaces to the sphere, an important class of methods has performed direct surface-to-surface registration.[37] In addition, methods using covariant partial differential equations attempt to produce surface-to-surface registrations that, in the continuous case at least, are independent of the intermediate spherical mappings used to impose grids on the surfaces.[34,38] In these mappings, a flow vector field in the surface coordinates is developed in which the differential operators are made covariant to the surface metrics, leading to surface registrations that are provably independent of the way the surfaces are gridded, so long as the surfaces are sufficiently finely sampled.

Within the grid generation field, there exist penalty functionals that will conserve a linear combination of length, orthogonality, and area so that semi-isometric flat maps of sections of the cortical surface can be generated. However, unless the surface is developable, it is not possible to conserve all three functionals. The brain surface mesh may be iteratively inflated by minimizing an energy functional that is related to metric distortion or geodesic lengths, creating a spherical mapping with low metric distortion.[39,40] Alternately, an initial simple mapping may be optimized by finding the minimum solution to an error functional that accounts for both area and angular distortion[41] or area and length distortion.[42] Semi-isometric flat maps of sections of the cortical surface may also be generated using a constrained optimization problem that accounts for both angles and area.[43] Such approaches are analogous to grid generation problems for surfaces using the compound functional method, and can be expanded to n dimensions in the general case.[44] In fact, equiareal mappings could be considered a subcase achievable by using only one of the three penalty functionals.[45]

In this paper, we propose to apply three algorithms to optimize spherical maps with respect to area distortion (and, secondarily, local metric distortion). The algorithms are unique and the problem is solved as an optimization problem to arrive at the minimum (distortion) solution. The method starts with initial spherical maps generated using a variety of previously developed methods. As a first step, the area distortion is minimized by finding the minimum solution to a nonlinear optimization problem based on an algorithm (the distort algorithm, Eq 8) that is directly related to area distortion. After the minimum solution is found, the spherical map is further optimized using more selective variants of all three algorithms. The resulting spherical map has improved distortion metrics compared to the original map. With respect to reparameterization of the spherical map into a spherical coordinate system, the optimized spherical maps result in a reparameterization that has significantly lower distance error values compared to the original map. The 3D distance error may be important in the field of morphometry, because if the original surface is not accurately approximated during reparameterization, some statistical power may be lost for shape and area analysis.

Methods

Minimizing Distortion

The definition of distortion is by no means established. Because of the nonheterogeneity of the distortion metrics used, it is feasible to select one metric to optimize. However, the optimization of one metric usually involves the degradation of another distortion metric, and this information is lost if other distortion metric values are not reported. Reporting a diverse set of distortion metrics for all resulting spherical maps can circumvent this.

Three standard distortion metrics include metric distortion, area distortion, and angle distortion.[44] The metric distortion metric is a universal measure that incorporates both area and angular distortion, whereas the area and angular distortion metrics selectively measure distortion in areas or angles, respectively. In the following discussion, the surface mesh is assumed to consist of triangles, but the metrics can be generalized to non-triangular meshes as well.

Metric distortion is a measure based on differences in distances between vertices. Because two triangles with three congruent sides must by definition be isometric, any deviation corresponds to distortion. Assume that there is a vertex $v_{o,i}$ in the original brain surface and its matching vertex on the unit sphere v_i. Let $d_{o,ij}$ and d_{ij} be the distances between the ith and jth vertices in the original brain and the spherical map, respectively.

The metric distortion is then defined as follows:

$$\Im_{\text{met}} = \frac{1}{N_v}\sum_{i=1}^{N_v}\left(\frac{1}{n(i)}\sum_{j\in n(i)}\left|d_{o,ij}-d_{ij}\right|/d_{ij}\right), \quad (1)$$

where N_v is the total number of vertices in the mesh and n are the neighboring vertices.[39,46] The metric distortion metric could be applied locally such that the set of neighboring vertices $n(i)$ includes only the 1-neighbors of the ith vertex, or it can be applied globally such that the neighboring vertices *n(i)* include all other vertices in the mesh; despite whether the measure is global or local, the optimal value signifying true isometry is zero. For global metric distortion calculations, it is necessary to select a random set of 1,000 vertices to reduce the computation time. For is subset of vertices, the same calculation shown in Equation 1 is applied.

Area distortion examines the areal difference for each triangle in the mesh. Assume that there is a triangle $t_{o,i}$ in the original brain surface and its spherical map equivalent t_i. We define area distortion of triangle t_i as follows:

$$\varepsilon_{i,\text{area}} = \log_{10}\left(\frac{A_o}{A}\frac{a_i}{a_{o,i}}\right). \quad (2)$$

Here, A_o and A are the total surface area of the brain mesh and the unit sphere mesh, whereas a_i and $a_{o,i}$ are the areas of the triangles $t_{o,i}$ in the brain mesh and t_i in the unit sphere mesh, respectively. The areas are normalized with respect to the total surface area of the mesh, allowing meshes of different physical dimensions to be compared. The area distortion metric ε_i has some interesting properties, in that it will create a distribution that is centered around zero, and a value of $+1$ means that a triangle is scaled by a factor of 10 compared to its equivalent triangle in the original mesh. The average area distortion of the entire mesh is defined as follows:

$$\Im_{\text{area}} = \frac{1}{N_t}\sum_{i=1}^{N_t}\left|\varepsilon_{i,\text{area}}\right|, \quad (3)$$

where N_t is the total number of triangles in the mesh.

To measure angle distortion, each of the three angles $\angle a_i$, $\angle b_i$, and $\angle c_i$ in triangle t_i need to be calculated and compared to the original three angles $\angle a_{o,i}$, $\angle b_{o,i}$, and $\angle c_{o,i}$ in triangle $t_{o,i}$. We then define the angular distortion for triangle t_i as follows:

$$\varepsilon_{i,angle} = \left|\angle a_i - \angle a_{o,i}\right| + \left|\angle b_i - \angle b_{o,i}\right| + \left|\angle c_i - \angle c_{o,i}\right|. \quad (4)$$

For this metric, the ideal value (eg, no angular distortion) is zero. The average angle distortion can then be calculated as follows:

$$\Im_{\text{angle}} = \frac{1}{3N_t}\sum_{i=1}^{N_t}\left|\varepsilon_{i,\text{angle}}\right|. \quad (5)$$

Weighted Algorithms for Area Distortion Correction

Weighted algorithms are applied directly upon the initial spherical map. Given a vertex v in the spherical map, each triangle adjacent to the vertex can be assigned a weight that can be used to adjust the position of the vertex. The center of each triangle t_j containing vertex v is found using the formula:

$$c_j = \left(\frac{x_v+x_r+x_s}{3}, \frac{y_v+y_r+y_s}{3}, \frac{z_v+z_r+z_s}{3}\right), \quad (6)$$

where r and s are the other two vertices in the triangle. One possible weighting scheme adjusts the vertex v so that the areas are more evenly distributed, such that the weight w_j of triangle t_j is

$$w_j = \frac{a_j}{A_v}, \quad (7)$$

where A_v is the total area of all triangles containing vertex v. The position of vertex v can then be updated as follows:

$$v'_{\text{area}} = \sum_{j=1}^{N} w_j c_j, \quad (8)$$

where N is the number of triangles containing vertex v. This weighting scheme could be considered as a form of smoothing in that it distributes area more equally among triangles, and it is beneficial only if the original mesh contains triangles of fairly uniform area or the spherical map has large area distortions. Applied indiscriminately to a mesh with nonuniform triangle sizes, the area distortion will eventually increase. However, the algorithm can be limited by calculating the local area distortion *post hoc*, and only updating the vertex v if local area distortion is reduced. The change in a patch of the spherical mesh after one iteration of this algorithm on the LB conformal map is shown in Figure 1C.

A modification of the above algorithm uses a weighting scheme based on the area distortion, as follows:

$$\chi_j = \frac{d_j}{D_v}. \quad (9)$$

Here, d_j is the area distortion of triangle t_j that includes vertex v, and D_v is the total distortion of all of the triangles that include vertex v. The area distortion d_j of triangle t_j can be found as follows:

$$d_j = \frac{a_j}{a_{o,j}}, \quad (10)$$

where a_j is the area of the triangle in the spherical map and $a_{o,j}$ is the area of the triangle in the original mesh. The updated vertex v'_{distort} can be found as follows:

$$v'_{\text{distort}} = \sum_{j=1}^{N} \chi_j c_j. \quad (11)$$

The advantage of this algorithm over the previous one is that it directly corrects for area distortion. It is also possible to calculate the local area distortion *post hoc*, updating the location of vertex v only if v'_{distort} is found to reduce local area distortion. The change in a patch of spherical mesh resulting from one iteration of this algorithm on the LB conformal map is shown in Figure 1D.

Ray-Tracing Algorithms for Metric Distortion Correction

An inherent property of triangles is that two triangles with three congruent sides must by default be isometric. Thus, by adjusting the length of each edge in the spherical map to be equal

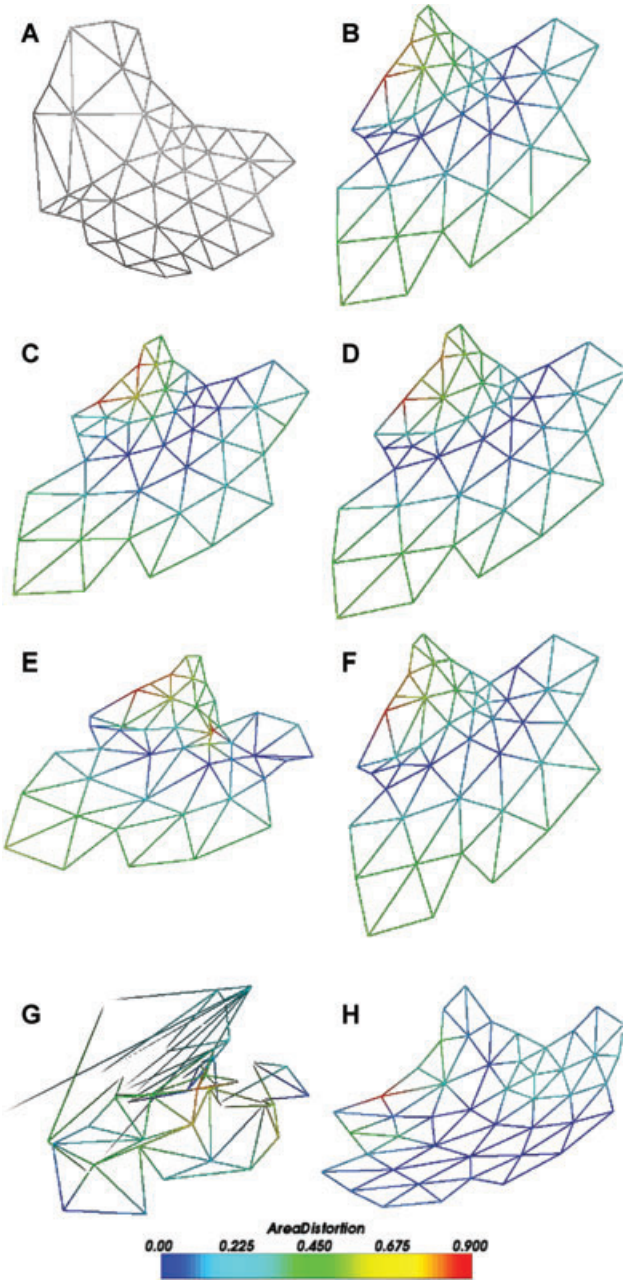

Fig 1. This figure shows a patch from the spherical mapping processed with a variety of algorithms for one iteration only. The entire map was processed and the patch was subsequently extracted. The original patch (A) is first processed using the Laplace-Beltrami operator (B) to generate a conformal map. The conformal map is then processed with only one iteration of the area algorithm (C), the distortion algorithm (D), the ray-tracing algorithm (E), or the ray-tracing algorithm selectively applied to large triangles (F). Without testing for triangle flips, the ray-tracing algorithm results in the mesh shown in (G). As a reference, a representative final patch is shown in (H).

to its corresponding edge in the original cortical surface map, the distortion in the spherical map should be reduced. This can be accomplished by tracing line segments in the spherical mesh along their vector direction such that the magnitude of the traced vector is equivalent to the length of the corresponding line segment in the original brain mesh.

Table 1. Iterative Optimization Pipeline

Correction	Algorithm	Options	Max iterations
Coarse	Distort (Eq 11)		100,000
Fine	Area (Eq 8)	Selective	1,000
	Ray-trace (Eq 13)	Selective	1,000
	Ray-trace (Eq 13)	Large triangles only	1,000
	Ray-trace (Eq 13)	Selective	1,000
	Distort (Eq 11)	Selective	1,000
	Ray-trace (Eq 13)	Selective	1,000

The algorithm traces all line segments adjacent to vertex v to update the position of the vertex such that metric distortion is reduced. If the directional vector $\boldsymbol{v}_j$ is the vector representation of a line segment in the spherical mesh that contains vertex v, then the ray-traced vector v'_j can be represented mathematically as follows:

$$v'_j = \left(\|v_j\| - \|v_{o,j}\|\right)\hat{v}_j. \tag{12}$$

Here, $\boldsymbol{v}_{o,j}$ is the vector representation of the corresponding line segment in the original brain mesh, and $\hat{v}_j$ is the unit vector along the direction of $\boldsymbol{v}_j$. The updated position of the vertex v is then

$$v'_{\text{ray}} = v + \frac{1}{N}\sum_{j=1}^{N} v'_j, \tag{13}$$

where N is the total number of line segments that are adjacent to vertex v. The ray-tracing function does not guarantee that the updated vertex positions lie upon the surface of the sphere, so a final step is to project the vertex onto the surface of the sphere. The change in a patch of the spherical mesh after one iteration of this algorithm on the conformal LB map is shown in Figures 1E–G.

Two major limitations of this algorithm need to be addressed to achieve a satisfactory solution. First, the updated vertex position can result in triangle flips (Fig 1G). This problem can be easily circumvented by testing whether the angles between the normals of neighboring triangles in the pre- and post-updated spherical mesh are larger than 1°, and excluding the vertex from the set of updated vertices if true (Fig 1E).

Second, the contribution to v'_{ray} from large triangles can overwhelm contributions from small triangles and can thus generate large metric distortions in small triangles. This is especially valid if the spherical map has large area distortion, such as the distortion that can be caused by the LB conformal map (which ignores area distortions to enforce angle conservation). To compensate for this limitation, the algorithm may be selectively applied only to vertices where the local area distortion is large (Fig 1F).

Finally, as earlier, it is also possible to calculate the local area distortion post hoc and update the location of the vertex only if local area distortion is reduced.

Optimization in Relation to Area Distortion

For meshes with large area distortion, empirical results demonstrate that the most effective algorithm for reducing area distortion is the distortion correction algorithm (Eq 11) (see "Results

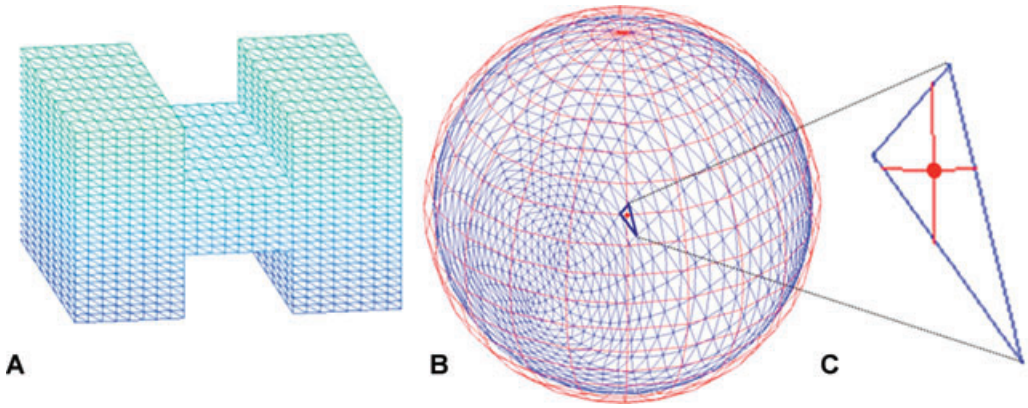

Fig 2. A surface is mapped to a sphere, then resampled onto regularly spaced grid. The original surface mesh (A) is mapped onto a sphere (B, blue). A regularly sampled sphere (B, red) is overlaid on top of this sphere. For each point in the regularly sampled grid (C, red), the intersecting triangle in the spherical mapping (C, blue) is found, and the barycentric coordinates within this triangle are calculated to obtain a coordinate of location within the original surface mesh.

and Discussion" section for the effect of each algorithm on distortion). If all vertices are included, this equation is essentially a nonlinear optimization problem whose ideal solution is achieved when the weights are equal to the inverse of the number of neighboring triangles. To arrive at the minimum solution, the problem can be solved iteratively, such that the surface mesh is only updated if the total area distortion of the mesh is significantly reduced. It is presumed that an initial spherical map that has more area distortion will require more iterations to arrive at the minimum solution than a spherical mapping with low initial area distortion.

After optimization using the distortion correction algorithm, the other algorithms are applied to further reduce area distortion in the order outlined in Table 1. This order was optimized empirically for computation speed and reduced distortion metrics. Generally, the "coarser" algorithms are applied first; these algorithms are "coarse" in that they result in relatively large changes in the distortion metrics. The mesh is then optimized with increasingly "finer" algorithms that make smaller changes in the distortion metrics. All initial spherical maps were processed using an identical algorithm pipeline.

Spherical Coordinate Reparameterization and Error Quantification

Using the original and optimized spherical maps, the surfaces are reparameterized using a spherical coordinate system, such

Table 2. Average Metric, Area, and Angular Distortion Metrics and Real Computation Time for 20 Central Surface Meshes

		Local metric distortion		Global metric distortion		Area distortion		Angular distortion		Time (s)	
CS	**IC**	**Mean**	**Δ**	**Mean**	**Δ**	Mean	**Δ**	**Mean**	**Δ**	**Mean**	**Δ**
LB		.3762	–	.3155	–	.3879	–	2.326	–	129.9	–
	√	.2372	−.1390	.2949	−.0206	.1677	−.2202	13.300	+10.974	8780.9	+8651.0
SI1		.3856	–	.2963	–	.2373	–	23.170	–	44.4	–
	√	.2372	−.1484	.2875	−.0088	.1299	−.1074	16.186	−6.984	899.3	+854.9
SI2		.2615	–	.2878	–	.1632	–	16.501	–	4523.5	–
	√	.2235	−.0380	.2874	−.0004	.1345	−.0287	14.417	−2.084	5115.2	+591.7

Δ: Change from uncorrected surface; IC: isometric correction; LB: Laplace–Beltrami; SI1: surface inflation method #1; SI2: surface inflation method #2.

Table 3. Average Metric, Area, and Angular Distortion Metrics and Real Computation Time for 20 White Matter Surface Meshes

		Local metric distortion		Global metric distortion		Area distortion		Angular distortion		Time (s)	
WM	**IC**	Mean	**Δ**	**Mean**	**Δ**	**Mean**	**Δ**	**Mean**	**Δ**	**Mean**	**Δ**
LB		.3932	–	.3285	–	.4235	–	2.044	–	104.2	–
	√	.2230	−.1702	.3022	−.0263	.1569	−.2466	13.003	+10.959	9243.5	+9139.3
SI1		.3506	–	.3079	–	.2199	–	22.523	–	44.4	–
	√	.2239	−.1267	.2993	−.0086	.1198	−.1001	15.915	−6.608	874.0	+829.6
SI2		.1988	–	.3066	–	.0769	–	15.903	–	4797.9	–
	√	.1983	−.0005	.3056	−.0010	.0760	−.0009	15.919	+.016	4960.7	+162.8

Δ: Change from uncorrected surface; IC: isometric correction; LB: Laplace–Beltrami; SI1: surface inflation method #1; SI2: surface inflation method #2.

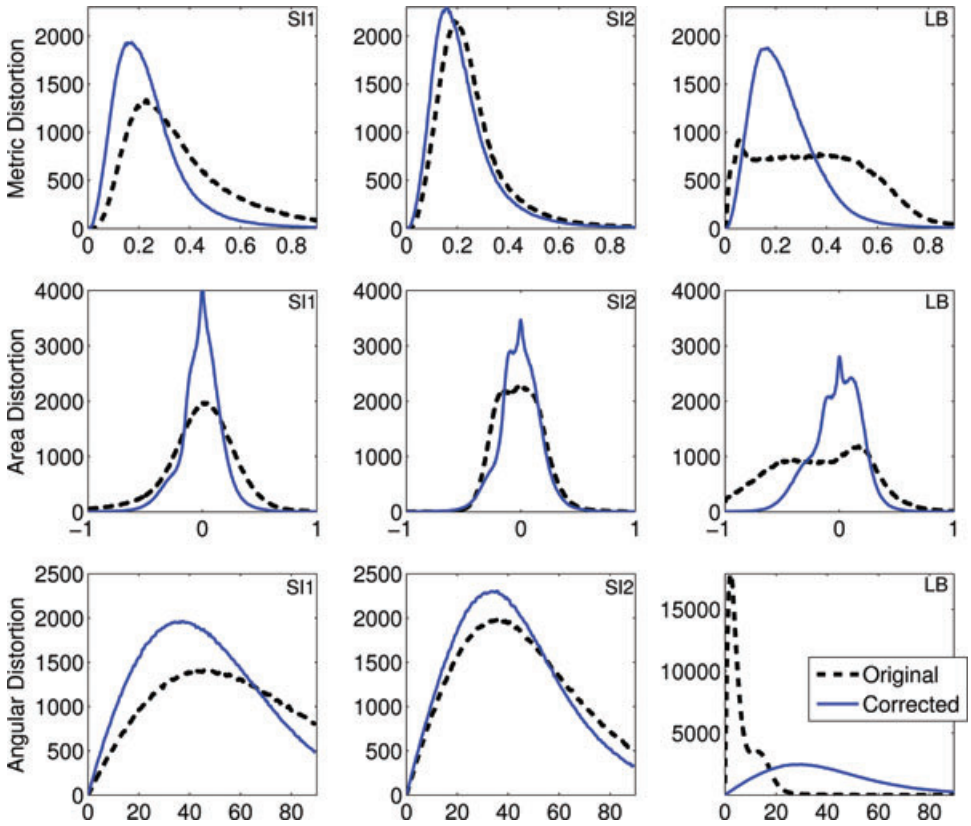

Fig 3. The average metric, area, and angular distortion histograms are shown here for 20 central surface meshes. The isometry correction process improves most profiles, except for the angular distortion for the Laplace-Beltrami initial mapping. LB: Laplace–Beltrami; SI1: surface inflation method #1; SI2: surface inflation method #2.

that the surfaces have regularly sampled points with respect to θ and ϕ, where θ is the colatitude and ϕ is the azimuthal coordinate. To accomplish this, points are generated from equally sampled values of θ and ϕ for all members in the sets, such that there are a varying number of points per set (128, 256, 512, or 1,024). For each regularly sampled spherical point, the bounding triangle on the cortical spherical map is found. Within that bounding triangle, a coordinate of location is approximated using barycentric coordinates, for example, the location of the regularly sampled point within the bounding triangle on the spherical map determines a certain set of barycentric coordinates, and these barycentric coordinates are then used within the corresponding triangle in the original cortical surface to find the cortical location. The result is a regularly sampled spherical map in which every point is associated with a coordinate related to the location on the original cortical surface (Fig 2). Near the poles (located along the north–south axis), the mesh has a higher resolution than at the equator. This increased point density at the poles may be avoided by regridding using refinement of Platonic solids; however, this additional step was not implemented for the results shown later.[47]

The reparameterized surfaces were then compared to the original brain surface mesh using the mean distance error and the Hausdorff distance. The minimum distance function $d(p,S')$ between a point $p \in X$ on the reparameterized mesh and the original brain surface S' can be defined as

$$d(p, S') = \min \| p - S' \| . \tag{14}$$

The mean distance error d_e is the average minimum distance between a set of points X and a surface S'

$$d_e = \frac{1}{N_p} \sum_{p \in X} d(p, S'), \tag{15}$$

where N_p is the number of points in the set of points X. The Hausdorff distance is simply the maximum distance error within the set of minimum distances:

$$d_H = \max\{d(p, S)\}, \tag{16}$$

There are two surfaces that are being compared, S and S'. It is key to note that the minimum distance from the set of points on surface S to the other surface S' is not equivalent to the minimum distance from the set of points on surface S' to surface S. When measuring the distance error from the reparameterized surface to the original brain surface, this will be referred to as the *forward* Hausdorff distance and mean distance error; in the other direction, it is the *reverse* Hausdorff distance and mean distance error.

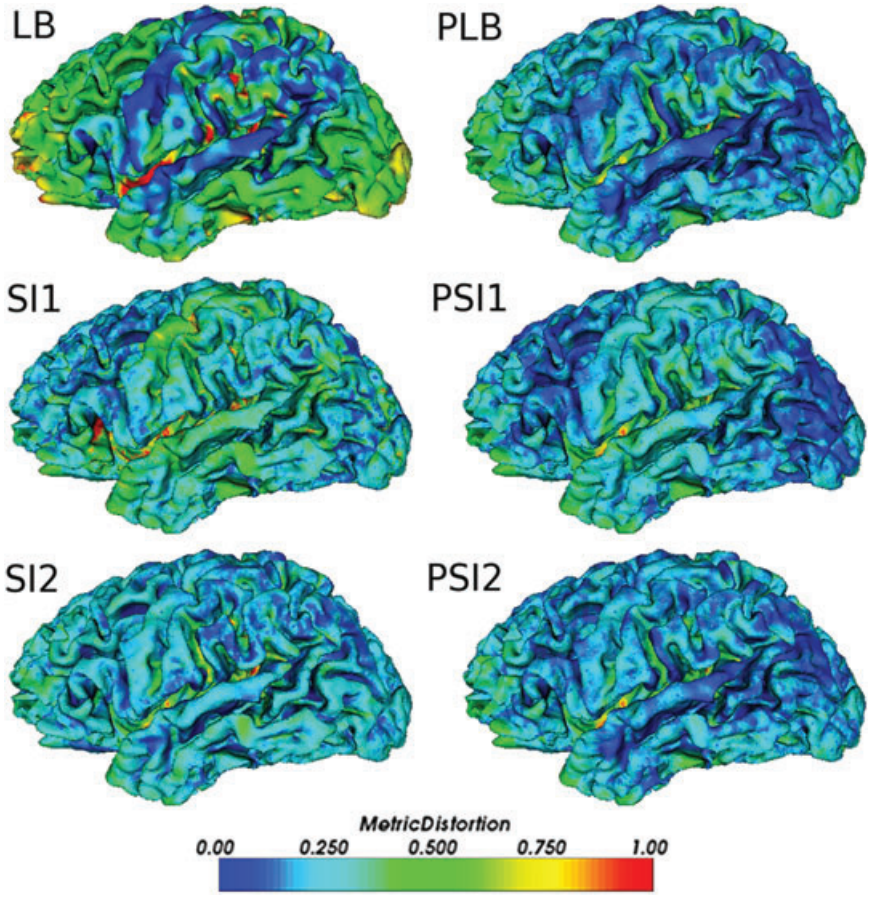

Fig 4. Shown is the distribution of the metric distortion across a sample central surface mesh. The isometry correction process (right column) reduces metric distortion for all initial spherical mapping methods (left column). For SI2, only the fine correction was used. P: isometry correction processed; LB: Laplace–Beltrami; SI1: surface inflation method #1; SI2: surface inflation method #2.

Sample Data

All results were generated using 10 healthy control subject brains. For the 10 control subjects (4 females and 6 males, mean age 35.3 years, SD ±11.3), T1-weighted images were obtained on a 1.5T Philips Gyroscan ACSII. There were 256 sagittal slices per scan (1 mm thickness, $T_R = 13$ ms, $T_E = 5$ ms, flip angle = 25°, field-of-view = 256 mm) with a matrix size of 256 × 256, resulting in an isotropic voxel size of 1 mm^3. All images were preprocessed using the processing pipeline (recon-all-all) included in FreeSurfer v4.0.5 (http://surfer.nmr.mgh.harvard.edu/) to obtain the initial white matter (WM) and pial surface meshes. Because there is a direct correspondence between the vertices in these two surfaces, these surfaces were averaged to obtain the central surface.

The initial spherical mappings were generated using one of three previously published methods: solving the LB operator with a Möbius transformation optimization[19]; inflating the brain surfaces using a smoothing operation (SI1)[48]; and inflating the brain surfaces while optimizing for metric distortion (SI2).[39] The isometry correction process was applied to both the WM and the central surface spherical maps for both the right and left hemispheres.

For all methods, the time to calculate the resulting spherical map mesh was obtained by running all analyses on an Apple Xserve with 2 Quad-Core Intel Xeon with 2.6 GHz running Mac OS X 10.5. No other programs were run at the same time while running the analysis.

Results and Discussion

Distortion Metrics Improve via Algorithmic Correction

The isometry correction process based on the three distortion correction algorithms outlined above creates a pseudo-isometric map of the cortical surface. Applied to the three initial spherical maps, the result is a spherical map that has significantly lower area and local metric distortion, with varying results on angular distortion and minimal cost in regards to computational time. There is low variability in the distortion results across subjects, indicating that the isometry correction process is fairly robust independent of the input spherical map. Computation times depend on both the mesh size (which for the sample data is an average of 126,000 points per mesh) and the average area distortion of the input spherical map.

The average area, angular, and local metric distortion values, as well as the real computation time, for the central surface

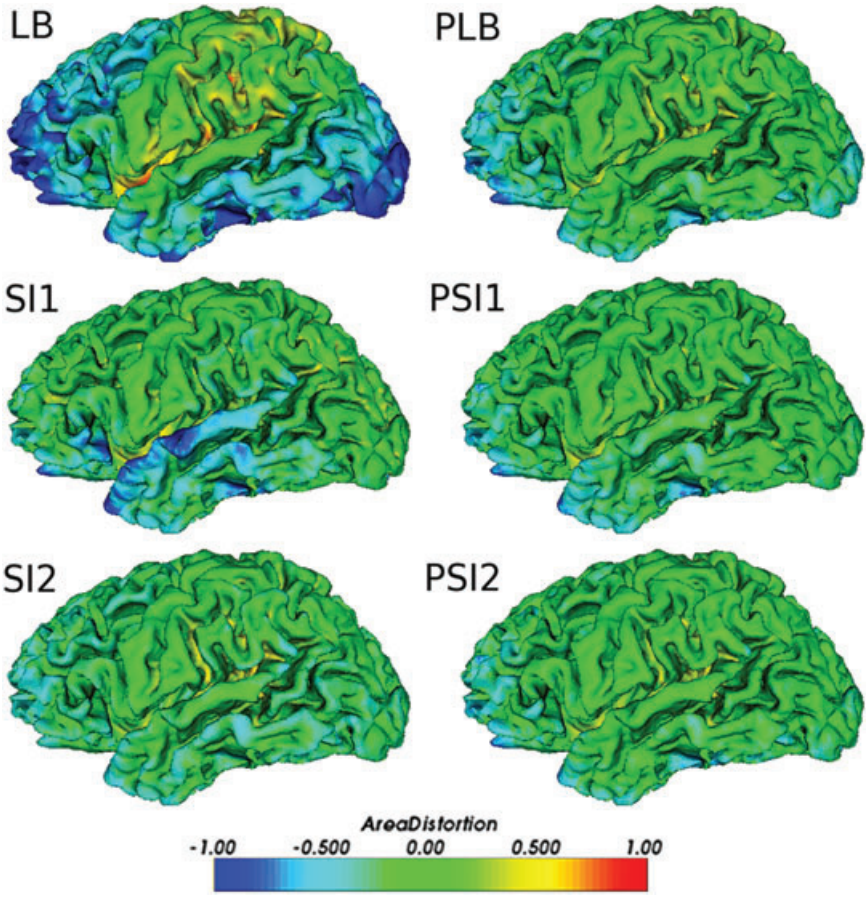

Fig 5. Shown is the distribution of the area distortion across a sample central surface mesh. The isometry correction process (right column) reduces area distortion for all initial spherical mapping methods (left column). For SI2, only the fine correction was used. P: isometry correction processed; LB: Laplace–Beltrami; SI1: surface inflation method #1; SI2: surface inflation method #2.

and WM surface are given in Tables 2 and 3, respectively. The initial spherical map that has fairly low metric distortion is the one generated using the SI2 method. In this case, the isometry correction process makes only minimal modification to the starting map, especially for the WM surface. However, for both the central and WM surfaces, the area and metric distortions are reduced. Conversely, the large initial area distortions of the LB conformal maps result in a significant increase in computation time compared to the other two initial maps.

The change in the distortion distribution due to the isometry correction process for the central surface is shown in Figure 3. In most cases, the isometry correction process results in an improved distortion profile. However, the LB conformal map had initially low angular distortion that was lost during the isometry correction process. The histogram profile is highly consistent for the mesh passed through the isometry correction process, independent of the initial spherical mapping method.

Figures 4–6 show the distribution of the metric, area, and angular distortion of the spherical map, mapped across the original central surface mesh. For the LB and SI1 mapping processes, both the coarse and fine corrections were used; the SI2 map was only processed with the fine correction. Under ideal circumstances, the distortion would be evenly distributed across the brain surface; however, it is not. With respect to angular distortion, the LB conformal map has very low angular distortion, but other methods create a map that has relatively large angular distortion along the gyri and not the sulci. The LB conformal map also compresses triangles at the rostral and caudal poles, as reflected in the large negative area distortion values located in these regions.

Most notably, the distortion in the final spherical map appears to be independent of the starting spherical map, as reflected numerically in the distortion metric values and visually in the histograms. Although there are an infinite number of solutions for mapping points onto a sphere, the minimum-distortion solution is a small subset of possible solutions. The similarity between the final mappings indicates that the isometry correction process converges toward a common minimum. The rate of convergence is initially fast, and then decreases as the spherical mapping solution approaches convergence.

We must also confirm that the cortical mapping onto the sphere does not have any large distortions. As Figure 7 shows, the isometry correction process dramatically reduces the distortion evident in the LB and SI1 mapping, while there is no significant change from the SI2 mapping. The LB conformal map devotes significantly more surface area to gyral regions than was originally present in the brain surface.

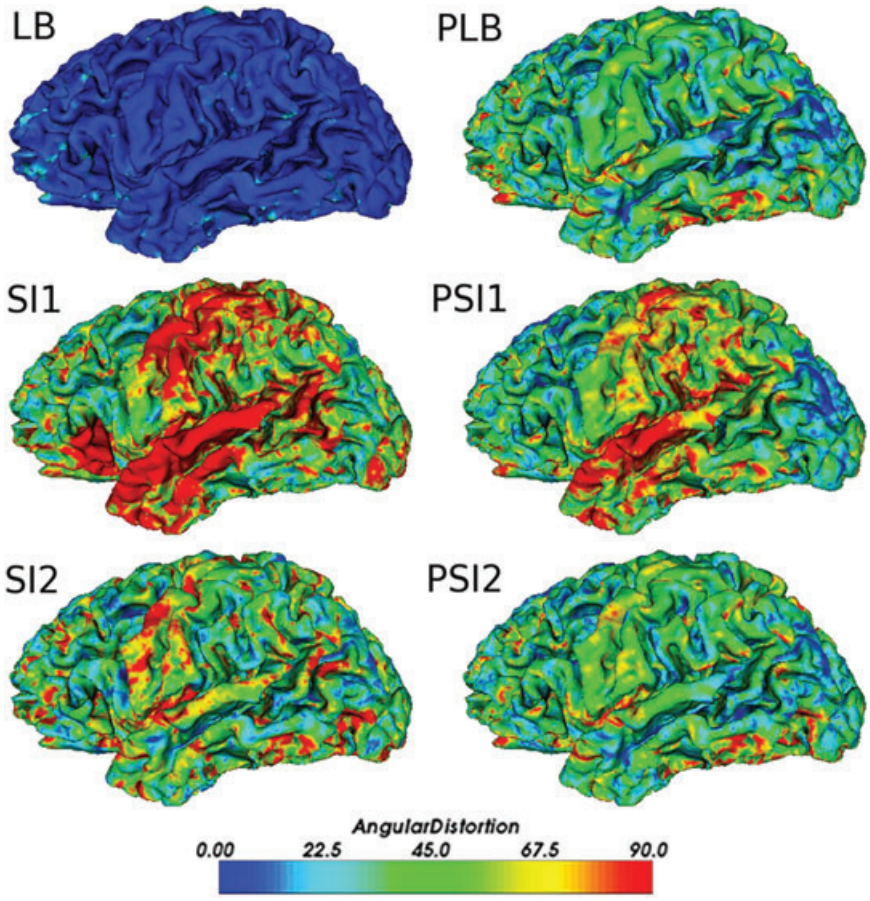

Fig 6. Shown is the distribution of the angular distortion across a sample central surface mesh. The isometry correction process (right column) reduces angular distortion for all initial spherical mapping methods (left column) except for LB. For SI2, only the fine correction was used. P: isometry correction processed; LB: Laplace–Beltrami; SI1: surface inflation method #1; SI2: surface inflation method #2.

Although the maps were of the central surface of one brain, the results generalize to the other central surface and WM maps. The isometry correction process generates a spherical map with low overall distortion, independent of the initial spherical mapping method.

Effects of Disparate Algorithms on Area and Angle Distortion

The comprehensive effects of each algorithm on the spherical mapping cannot be fully understood due to the complex nature of the mesh being acted upon. However, it is worthwhile to attempt to tease out the peculiar effects of each algorithm on the spherical mappings by passing a map through 1,000 iterations of each algorithm alone and measuring the resulting area and angular distortion (Fig 8). The LB conformal map was chosen as the initial map due to its relatively high initial metric distortion.

The ray-tracing algorithm (Eq 13) and its large-triangle-only variant produced maps that had approximately the same area distortion but much larger angular distortion compared to the original LB conformal map. An examination of the maps reveals that this is due precisely to the complex nature of the mesh being acted upon. Some triangles are corrected at a high cost to neighboring triangles. The ray-tracing algorithm was indeed found to perform well only when the area and angular distortion were already fairly low.

The two weighted algorithms (Eqs 8 and 11) generated maps that had significantly lower area distortion than the original LB conformal map, with the distortion variant (Eq 11) outperforming the area-only algorithm (Eq 8) in both metrics. In general, the distortion variant (Eq 11) was found to be the best solution for generating a spherical map from the LB conformal map in terms of computation speed and distortion metrics, compared to other algorithms.

Reparameterization Accuracy as a Function of Distortion and Resolution

Generally, the forward Hausdorff distance and mean distance error metrics measure how well the reconstructed surface matches the original surface mesh; the reverse Hausdorff distance and mean distance error indicate how much information from the original surface mesh was retained in the reconstruction. It is therefore expected that the forward metrics may increase as a function of resolution, since there are simply more points in the mesh that will have potentially larger distance errors. However, these measures should be extremely small values, which was experimentally confirmed; the two metrics

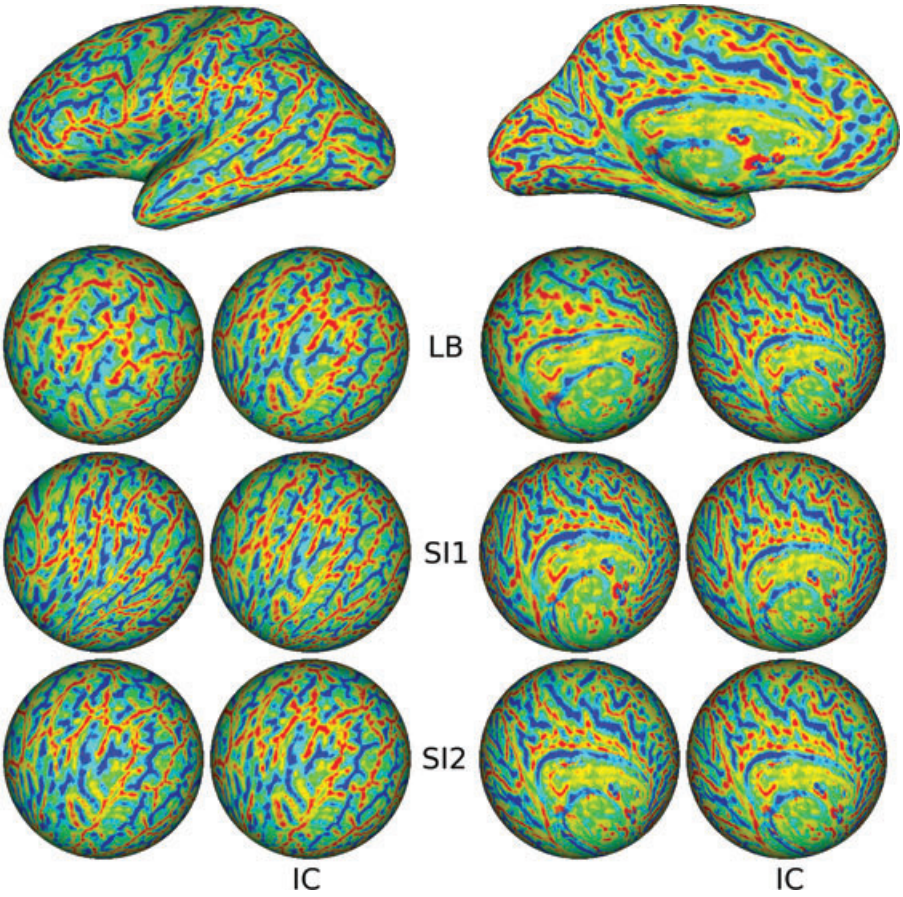

Fig 7. Cortical mappings onto the spherical mesh are shown on the sphere for the lateral (left) and medial (right) cortical central surfaces for one subject. The top row shows the inflated surface as a reference. The surface achieved via the isometry correction process is similar, independent of the initial spherical mapping. For the SI2 method, there is almost no change, since the original mapping had low distortion. IC: isometry correction; LB: Laplace–Beltrami; SI1: surface inflation method #1; SI2: surface inflation method #2.

are on the order of nanometers rather than millimeters (Figs 9 and 10).

For the reverse metrics, it is expected that a higher resolution mesh will decrease these values, which was found to be the case (Figs 9 and 10). The mean distance error can be considered to be a more critical measure than the Hausdorff distance, because the Hausdorff distance is the absolute maximum rather than an overall measure for the entire surface mesh. A large mean distance error indicates that geometric information from the original cortical surface mesh is not adequately represented in the reparameterized mesh.

For both the central and WM surfaces, the reverse mean distance error decreased if the isometry correction process was applied; for the SI2 method, there was only a slight decrease in this measure (Tables S1 and S2). The reverse Hausdorff distance also decreased for all cases, with the one exception of SI2 for the CS at low resolutions. It can be assumed that this occurred due to the way that the SI2 mesh was created. The surface was inflated while minimizing a squared edge length error. Because the value is squared, outliers are punished more so than in the isometry correction process, which uses an error function that is directly proportional to the length error. This can be translated into fewer distance error outliers during the

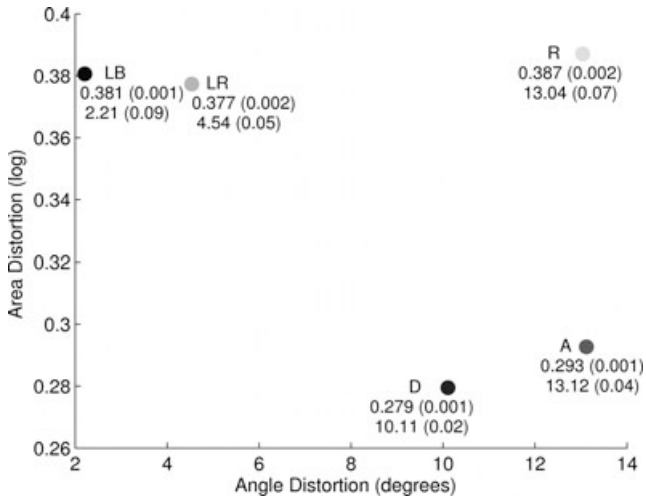

Fig 8. A scatter plot of average area distortion metrics versus average angular distortion metrics is shown here, for central surface spherical maps using just a single algorithm over 1,000 iterations. The average area and angular distortion metrics (with standard error of the mean) are included. LB: Laplace–Beltrami; A: area; D: distort; R: ray-trace; LR: ray-trace for large triangles only.

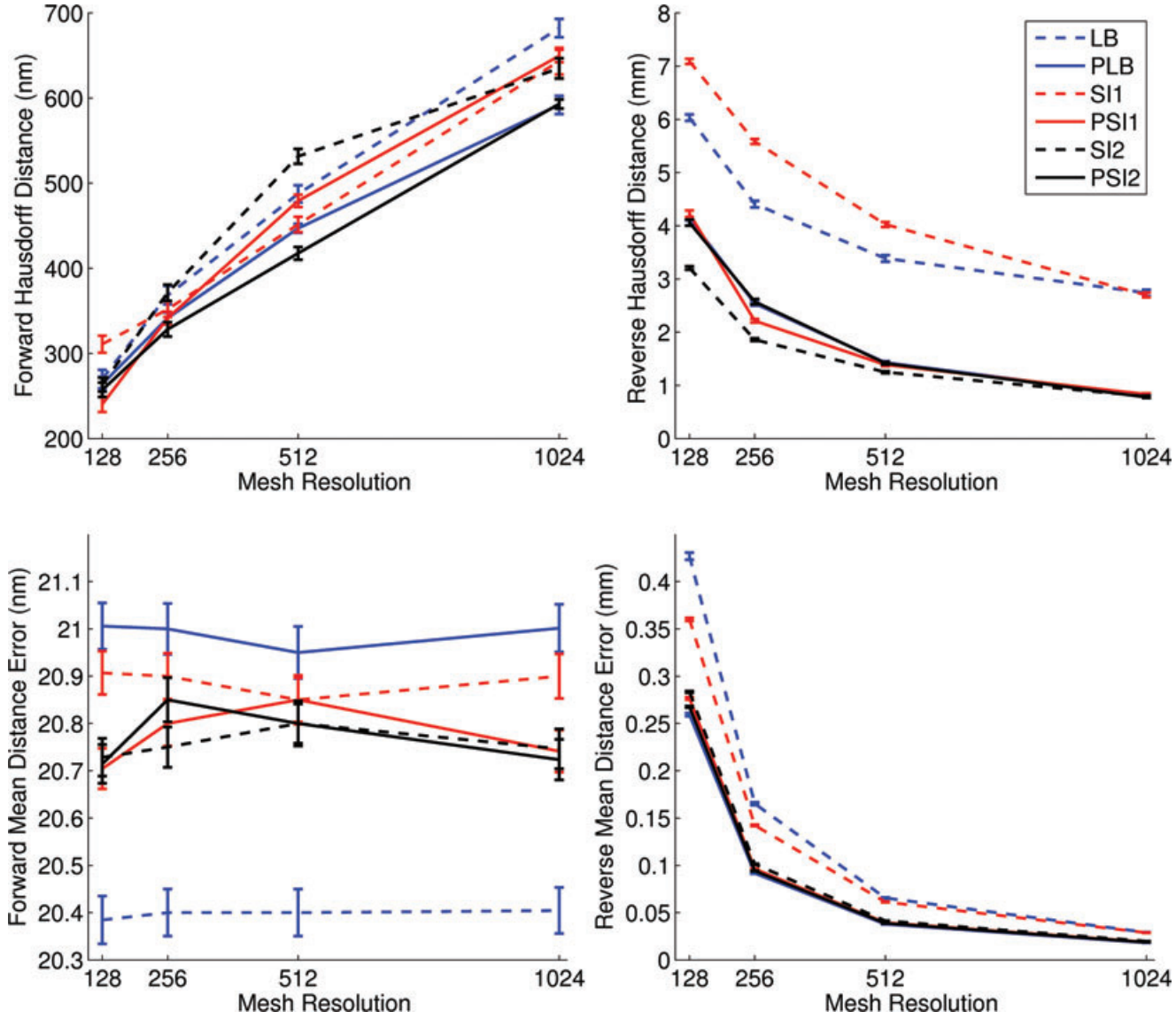

Fig 9. For the central surface, the average Hausdorff distance and mean distance error change as a function of mesh resolution. For the reverse Hausdorff distance, the PLB and PSI2 methods are almost equivalent; for the mean distance error, the PLB, PSI1, SI2, and PSI2 methods overlap for most mesh resolutions. Error bars show the standard error of the mean for the 20 meshes. P: isometry correction processed; LB: Laplace–Beltrami; SI1: surface inflation method #1; SI2: surface inflation method #2.

reparameterization process, which will have an effect on the reverse Hausdorff distance (a maximization term) but not on the reverse mean distance error. Instead, the mean distance error is minimized if the distortion is minimized, which was found to be the case, because the isometry correction process reduces both the distortion metrics and the reverse mean distance errors.

Conclusion

Our isometry correction process significantly decreases the distortion of spherical maps using a combination of three original algorithms. The starting spherical map was generated using one of three common methods: a conformal map obtained by solving a partial differential equation involving the LB operator of the surface coordinates and optimized with a Möbius transformation, iteratively smoothing and inflating the brain surface mesh until a spherical shape is obtained, and inflating the brain surface mesh while minimizing a metric distortion energy functional. Independent of the method used to generate the starting spherical map, the map that resulted after processing with the isometry correction algorithms exhibited lower metric and area distortion, at relatively minimal cost to angular distortion.

The analyses were conducted on the central and WM surfaces. Conceivably, there are three potential surfaces that can be analyzed: the WM surface, the pial surface, and the central surface. The central surface can be constructed by averaging the pial and WM surfaces, or by extracting it directly from the volumetric data. Generally, the pial surface tends to have more pronounced folds, whereas the WM surface tends to have

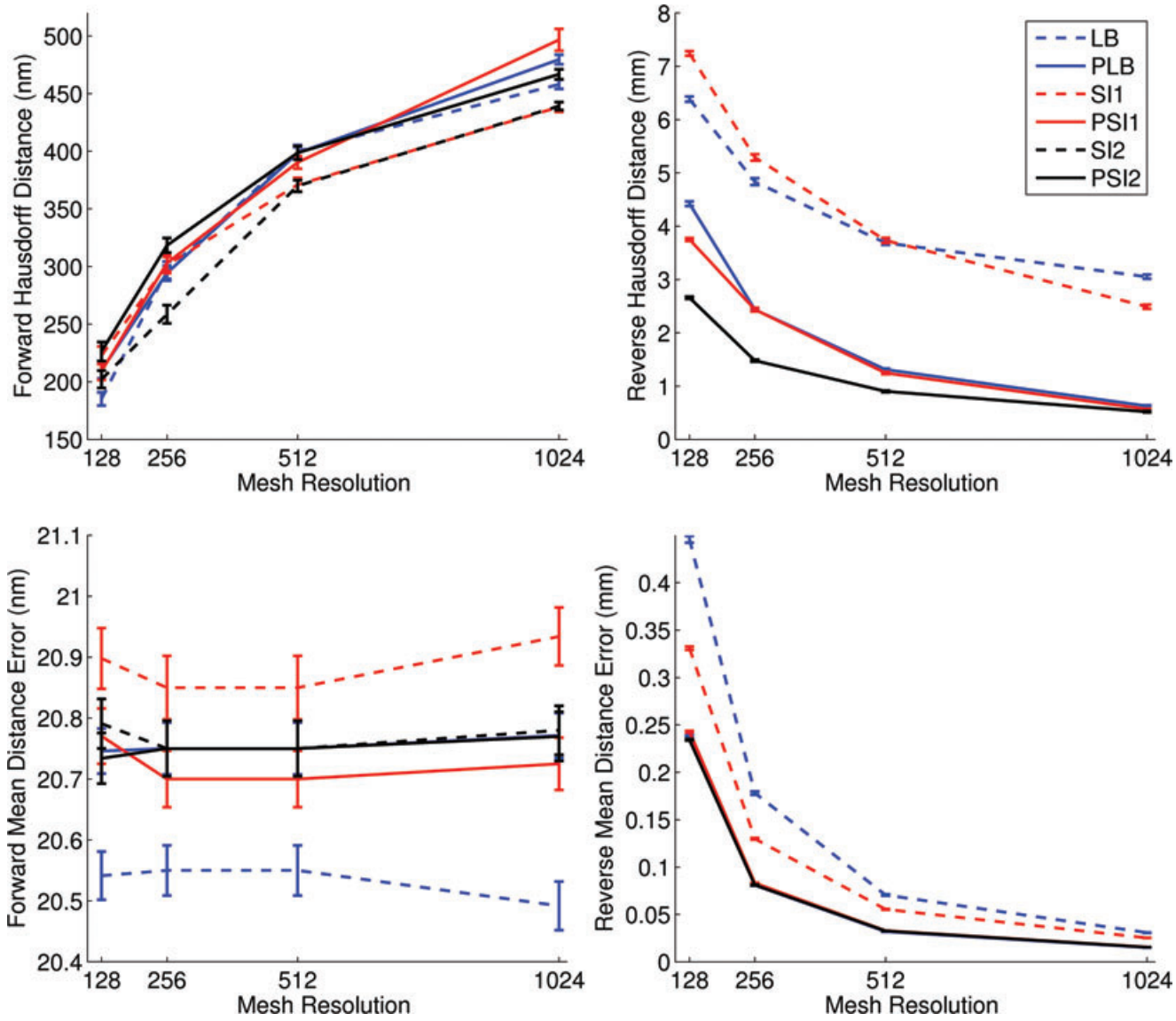

Fig 10. For the WM surface, the average Hausdorff distance and mean distance error change as a function of mesh resolution. For the reverse mean distance error, the PLB, PSI1, SI2, and PSI2 methods overlap for most mesh resolutions. Error bars show the standard error of the mean for the 20 meshes. P: isometry correction processed; LB: Laplace–Beltrami; SI1: surface inflation method #1; SI2: surface inflation method #2.

higher average curvature, or a rougher surface. We chose to focus on the central surface to have a midway representation between these two extremes. The central surface might represent the cortical ribbon more accurately than surfaces along either the inner or outer boundary,[15] because both sulci and gyri are better defined. However, to confirm the generality of the isometry correction process, the numerical results for the WM surfaces were also included. These results demonstrate a more significant correction via the isometry correction process than was observed for the central surface.

Each algorithm used in the processing pipeline has an antecedent, and elucidating these relationships may help future research. For instance, the weighted algorithm that updates the vertices based solely on area is related to smoothing functions, because by default it creates a distribution of triangle areas that is more uniform. An improved variant of this algorithm would be directly related to area distortion, and it was experimentally confirmed that choosing a weight based on area distortion results in an improved outcome.

A class of algorithms that could be considered antecedent to the ray-tracing algorithm is those that calculate energy functions that minimize metric distortion.[39,49] However, metric distortion is an indefinite term. Some previous definitions include the variance of the distance error extremes, the square-mean error of distance, or the direct distance error. Furthermore, the distance error can be local or global, in which the latter incorporates the geodesic distance error of each vertex to all other vertices in the mesh. It may be of interest to elucidate one algorithm from this class in detail. The FreeSurfer suite reduces distortion by calculating an energy functional that must be

minimized. The energy functional includes a value representing a form of local metric distortion as well as a spring force to drive surface inflation, where the metric distortion term is the mean-squared local distance error. Minimizing this energy functional during surface inflation produces a surface with low distortion but at relatively high computational cost. In contrast, the ray-tracing algorithm is applied iteratively and potentially independently of the mesh distortion, thus reducing the computation time.

Certainly, it is optimal to reduce the global metric distortion, which would minimize the change in geodesic distance between prominent surface features.[50] The computational cost of computing the global metric distortion naturally restricts the direct use of this metric when inflating the surface or mapping to a sphere. Theoretically, the local overall reduction of metric distortion inherently leads to low global metric distortion, yet forthcoming developments in computational power may permit a more direct application of global metric distortion in spherical mapping.

Reparameterization of the spherical mapping was improved with respect to distance error values if the area distortion of the spherical mapping was reduced. A related problem in spline theory optimizes this criterion (eg, distance error) directly by adjusting the location of the reparameterized points. If the goal is to maximize the surface fidelity using a fixed number of points, the best mapping will be one that is adaptive to the local curvature of the surface, for example, flatter areas of the surface will be sampled using fewer points, and the point density will increase in high-curvature regions. An equiareal mapping achieves this approximately, which is reflected in the decreased distance errors during re-parameterization.

This work was supported by the following grants from the German Bundesministerium für Bildung und Forschung: BMBF 01EV0709 and BMBF 01GW0740.

Funding sources: BMBF 01EV0709, BMBF 01GW0740.

References

1. Memoli F, Sapiro G, Thompson P. Implicit brain imaging. *NeuroImage* 2004;23(Suppl 1):S179-S188.
2. Thompson PM, MacDonald D, Mega MS, et al. Detection and mapping of abnormal brain structure with a probabilistic atlas of cortical surfaces. *J Comput Assist Tomogr* 1997;21(4):567-581.
3. Thompson PM, Schwartz C, Toga AW. High-resolution random mesh algorithms for creating a probabilistic 3D surface atlas of the human brain. *NeuroImage* 1996;3:19-34.
4. Narr KL, Bilder RM, Kim S, et al. Abnormal gyral complexity in first-episode schizophrenia. *Biol Psychiatry* 2004;55(8):859-867.
5. Luders E, Narr KL, Thompson PM, et al. Gender differences in cortical complexity. *Nat Neurosci* 2004;7(8):799-800.
6. Thompson PM, Schwartz C, Lin RT, et al. Three-dimensional statistical analysis of sulcal variability in the human brain. *J Neurosci* 1996;16(13):4261-4274.
7. Desai R, Liebenthal E, Possing ET, et al. Volumetric vs. surface-based alignment for localization of auditory cortex activation. *NeuroImage* 2005;26(4):1019-1029.
8. Hinds OP, Rajendran N, Polimeni JR, et al. Accurate prediction of V1 location from cortical folds in a surface coordinate system. *NeuroImage* 2008;39(4):1585-1599.
9. Fischl B, Sereno MI, Tootell RBH, et al. High-resolution intersubject averaging and a coordinate system for the cortical surface. *Hum Brain Mapp* 1999;8(4):272-284.
10. Thompson PM, Toga AW. A surface-based technique for warping three-dimensional images of the brain. *IEEE Trans Med Imaging* 1996;15(4):402-417.
11. Luders E, Thompson PM, Narr KL, et al. A curvature-based approach to estimate local gyrification on the cortical surface. *NeuroImage* 2006;29(4):1224-1230.
12. Schaer M, Cuadra MB, Tamarit L, et al. A surface-based approach to quantify local cortical gyrification. *IEEE Trans Med Imaging* 2008;27(2):161-170.
13. Han X, Jovicich J, Salat D, et al. Reliability of MRI-derived measurements of human cerebral cortical thickness: the effects of field strength, scanner upgrade and manufacturer. *NeuroImage* 2006;32(1):180-194.
14. Fischl B, Dale AM. Measuring the thickness of the human cerebral cortex from magnetic resonance images. *Proc Natl Acad Sci USA* 2000;97(20):11050-11055.
15. Van Essen DC, Drury HA, Dickson J, et al. An integrated software suite for surface-based analyses of cerebral cortex. *J Am Med Inform Assoc* 2001;8(5):443-459.
16. Floater MS, Hormann K. Surface parameterization: a tutorial and survey. In: Dodgson N, Floater MS, Sabin M, eds. *Advances in Multiresolution for Geometric Modelling*. Vol IV. Berlin Heidelberg: Springer; 2005:157-186.
17. Schwartz EL. Spatial mapping in the primate sensory projection: analytic structure and relevance to perception. *Biol Cybern* 1977;25(4):181-194.
18. Angenent S, Haker S, Tannenbaum A, et al. On the Laplace-Beltrami operator and brain surface flattening. *IEEE Trans Med Imaging* 1999;18(8):700-711.
19. Tosun D, Rettmann ME, Prince JL. Mapping techniques for aligning sulci across multiple brains. *Med Image Anal* 2004;8(3):295-309.
20. Lui LM, Wang Y, Chan TF, et al. Automatic landmark tracking applied to optimize brain conformal mapping. *Proceedings of the IEEE International Symposium on Biomed Imaging*. Arlington, VA, 2006.
21. Lui LM, Wang YL, Chan TF, et al. Brain anatomical feature detection by solving partial differential equations on a general manifold. *J Discrete Cont Dyn Syst, Ser B* 2007;7(3):605-618.
22. Lui LM, Wang Y, Chan TF, et al. Landmark constrained genus zero surface conformal mapping and its application to brain mapping research. *Appl Numer Math* 2007;57(5-7):847-858.
23. Gu X, Wang Y, Chan TF, et al. Genus zero surface conformal mapping and its application to brain surface mapping. *IEEE Trans Med Imaging* 2004;23(8):949-958.
24. Wang Y, Chiang M-C, Thompson PM. 3D surface matching with mutual information and Riemann surface structures. *Comput Graph Imaging*. Honolulu, HI; 2005:94-99.
25. Joshi AA, Shattuck DW, Thompson PM, et al. Cortical surface parameterization by p-harmonic energy minimization. *Proceedings of the IEEE International Symposium of Biomed Imaging*. pp. 428-431. Arlington, VA, 2004.
26. Joshi AA, Shattuck DW, Thompson PM, et al. Surface-constrained volumetric brain registration using harmonic mappings. *IEEE Trans Med Imaging* 2007;26(12):1657-1669.
27. Hurdal MK, Stephenson K. Cortical cartography using the discrete conformal approach of circle packings. *NeuroImage* 2004;23(Suppl 1):S119-S128.
28. Wang Y, Gu X, Chan TF, et al. Multivariate tensor-based brain anatomical surface morphometry via holomorphic one-forms. *Med Image Comput Comput Assist Interv* 2009;5761:337-344.
29. Wang Y, Gu X, Chan TF, et al. Brain surface conformal parameterization with the Ricci flow. *Proc IEEE Int Symp Biomed Imaging*. pp. 1312-1315. Arlington, VA, 2007.

30. Wang Y, Gu X, Chan TF, et al. Brain mapping with the Ricci flow conformal parameterization and multivariate statistics on deformation tensors. *Proceedings of the 2nd MICCAI Workshop on Mathematical Foundations of Computational Anatomy*. pp. 36-47. New York, NY, 2008.
31. Wang Y, Gu X, Chan TF, et al. Brain surface conformal parameterization with algebraic functions. *Med Image Comput Comput Assist Interv* 2006;9(Pt 2):946-954.
32. Wang Y, Gu X, Chan TF, et al. Brain surface conformal parameterization with the slit mapping. *Proceedings of the IEEE International Symposium on Biomed Imaging*. pp. 448-451. Paris, 2008.
33. Wang Y, Gu X, Chan TF, et al. Shape analysis with conformal invariants for multiply connected domains and its application to analyzing brain morphology. *NeuroImage* 2009;47(Suppl 1):S39-S41.
34. Thompson PM, Hayashi KM, Sowell ER, et al. Mapping cortical change in Alzheimer's disease, brain development, and schizophrenia. *NeuroImage* 2004;23(Suppl 1):S2-S18.
35. Leow A, Yu CL, Lee SJ, et al. Brain structural mapping using a novel hybrid implicit/explicit framework based on the level-set method. *NeuroImage* 2005;24(3):910-927.
36. Wang Y, Lui LM, Chan TF, et al. Optimization of brain conformal mapping with landmarks. *Med Image Comput Comput Assist Interv* 2005;8(Pt 2):675-683.
37. Shi Y, Thompson PM, Dinov I, et al. Direct cortical mapping via solving partial differential equations on implicit surfaces. *Med Image Anal* 2007;11(3):207-223.
38. Thompson PM, Hayashi KM, de Zubicaray GI, et al. Detecting dynamic and genetic effects on brain structure using high-dimensional cortical pattern matching. *Proceedings of the IEEE International Symposium on Biomed Imaging*. pp. 473-476. Washington, DC, 2002.
39. Fischl B, Sereno MI, Dale AM. Cortical surface-based analysis. II. Inflation, flattening, and a surface-based coordinate system. *NeuroImage* 1999;9(2):195-207.
40. Carman GJ, Drury HA, Van Essen DC. Computational methods for reconstructing and unfolding the cerebral cortex. *Cereb Cortex* 1995;5(6):506-517.
41. Kruggel F. Robust parametrization of brain surface meshes. *Med Image Anal* 2008;12(3):291-299.
42. Shen L, Makedon F. Spherical parameterization for 3D surface analysis in volumetric images. *Proceedings of the International Conference on Information Technology: Coding and Computing*. Vol 2, pp. 643-649. Las Vegas, NV, 2004.
43. Timsari B, Leahy RM. Optimization method for creating semi-isometric flat maps of the cerebral cortex. *SPIE Symposium on Medical Imaging 2000: Image Processing*. Vol. 3979, pp. 698-708. San Diego, CA, 2000.
44. Liseikin VD. *Grid Generation Methods*. Heidelberg: Springer-Verlag; 1999
45. Tinoco-Ruiz J-G, Barrera-Sanchez P, Cortes-Medina A. Some properties of area functionals in numerical grid generation. *Proceedings of the 10th International Meshing Roundtable*. Newport, pp. 43-54. Beach, CA, 2001.
46. Ju L, Stern J, Rehm K, et al. Cortical surface flattening using least square conformal mapping with minimal metric distortion. *Proceedings of the IEEE International Symposium on Biomed Imaging*. pp. 77-80. Arlington, VA, 2004.
47. MacDonald D. *A method for identifying geometrically simple surfaces from three dimensional images*. Montreal: School of Computer Science, McGill Unversity, 1998.
48. Drury HA, Van Essen DC, Anderson CH, et al. Computerized mappings of the cerebral cortex: a multiresolution flattening method and a surface-based coordinate system. *J Cogn Neurosci* 1996;8(1):1-28.
49. Praun E, Hoppe H. Spherical parametrization and remeshing. *ACM Trans Graph* 2003;22(3):340-349.
50. Schwartz EL, Shaw A, Wolfson E. A numerical solution to the generalized mapmaker's problem: flattening nonconvex polyhedral surfaces. *IEEE Trans Pattern Anal Machine Intell* 1989;11(9):1005-1008.

Supporting Information

Additional supporting information may be found in the online version of this article:

Table S1. Mean distance error and Hausdorff distances for 20 central surface meshes

Table S2. Mean distance error and Hausdorff distances for 20 white matter surface meshes

Please note: Wiley-Blackwell are not responsible for the content or functionality of any supporting materials supplied by the authors. Any queries (other than missing material) should be directed to the corresponding author for the article.